Journal of Magnetic Resonance 193 (2008) 168–176

Contents lists available at ScienceDirect

Journal of Magnetic Resonance

journal homepage: www.elsevier.com/locate/jmr

Implementation of controlled phase shift gates and Collins version of Deutsch–Jozsa algorithm on a quadrupolar spin-7/2 nucleus using non-adiabatic geometric phases

T. Gopinath *, Anil Kumar

NMR Quantum Computing and Quantum Information Group, Department of Physics, and NMR Research Centre, Indian Institute of Science, Yeshwanthpur, Bangalore, Karnataka 560012, India

ARTICLE INFO

Article history:
Received 20 November 2007
Revised 12 April 2008
Available online 16 April 2008

Keywords:
Quantum computing
Quadrupolar nucleus
Non-adiabatic geometric phase

ABSTRACT

In this work controlled phase shift gates are implemented on a qaudrupolar system, by using non-adiabatic geometric phases. A general procedure is given, for implementing controlled phase shift gates in an '*N*' level system. The utility of such controlled phase shift gates, is demonstrated here by implementing 3-qubit Deutsch–Jozsa algorithm on a spin-7/2 quadrupolar nucleus oriented in a liquid crystal matrix.

Published by Elsevier Inc.

1. Introduction

The use of quantum systems for information processing was first introduced by Benioff [1]. In 1985 Deutsch described quantum computers which exploit the superposition of multi particle states, thereby achieving massive parallelism [2]. Researchers have also studied the possibility of solving certain types of problems more efficiently than can be done on conventional computers [3–5]. These theoretical possibilities have generated significant interest for experimental realization of quantum computers [6,7]. Several techniques are being exploited for quantum computing and quantum information processing, including nuclear magnetic resonance (NMR) [8,9].

NMR has played a leading role for the practical demonstration of quantum gates and algorithms [8–14]. Most of the NMR quantum information processing (QIP) experiments have utilized spin-1/2 systems having indirect spin–spin couplings (scalar J couplings), known as weakly J coupled systems. In such systems, single qubit gates are obtained by selectively manipulating the qubits by applying qubit (spin) selective pulses, and multi-qubit gates are obtained by spin–echo methods [10–14]. Price et al. have given a systematic procedure for implementing multi-qubit gates [15–17]. It is interesting to note that, a new class of algorithms, known as adiabatic algorithms have also been proposed and successfully implemented in NMR [18–20]. Such algorithms start from a suitable initial state and by evolution under slowly time varying Hamiltonian, reach the desired output state. Recently NMR QIP has been demonstrated in quadrupolar and dipolar coupled systems, obtained by orienting the molecules in liquid crystal media [21,22]. In case of homo nuclear dipolar coupled systems, spins are often strongly coupled and hence cannot be addressed individually [23]. However the 2^n eigen states of an n-coupled system, are collectively treated as an n-qubit system [21,23,37]. Similarly for quadrupolar systems (spin > 1/2), individual spins are treated as a multi-qubit system [22,24–35]. Resolved resonance lines provide access to the full Hilbert space of 2^n dimension [22,24].

Quadrupolar interaction arises for nuclei with spin > 1/2, resulting from the electrostatic interaction between nucleus and electric charge distributions [39]. In liquids the quadrupolar interaction which is anisotropic (orientation-dependent), is averaged to zero, due to rapid isotropic reorientations of the molecules and in rigid solids one obtains broad lines or powder pattern [39]. In molecules partially oriented in anisotropic media, like liquid crystals, molecules attain partial orientational order but no translational order, such that intra molecular anisotropic interactions survive, but are scaled down by the order parameter of the liquid crystal, yielding finite number of sharp NMR resonances [40]. In the presence of strong magnetic field, Zeeman interaction can be assumed to be much stronger than quadrupolar interaction, as a consequence quadrupolar Hamiltonian can be truncated by Zeeman Hamiltonian [39,40]. The total Hamiltonian consists of Zeeman term $H_z = \omega_o I_z$ and a quadrupolar coupling term $H_Q (= H_Q^1 + H_Q^2 + \cdots)$, where $\omega_o = -\gamma B_o$ is the resonance frequency and H_Q^i is the ith order quadrupolar Hamiltonian which is inversely proportional to $(i-1)$th power of ω_o. Under high magnetic fields and reduced

* Corresponding author.
E-mail address: gopi@umn.edu (T. Gopinath).

1090-7807/$ - see front matter Published by Elsevier Inc.
doi:10.1016/j.jmr.2008.04.018

quadrupolar coupling (by nearly three orders of magnitude) due to reduced order parameter in a liquid crystal medium, only H_Q^1 which is independent of ω_o, contributes to H_Q:

$$H = H_z + H_Q = H_z + H_Q^1 = \omega_o I_z + A_Q(3I_z^2 - I^2),$$
$$A_Q = \frac{2\pi e^2 qQ}{[4I(2I-1)]}\left\langle\left[\frac{1}{2}(3\cos^2(\alpha)-1) + \frac{\eta}{2}\cos(2\alpha)\sin^2(\beta)\right]\right\rangle, \quad (1)$$

where eq and eQ, respectively represent electric field gradient and nuclear electric quadrupole moment, A_Q is the time averaged or effective quadrupolar coupling constant, α and β are determined by the orientation of the priciple axis frame (PAF) of the molecule with respect to the laboratory frame z-axis (B_o field direction) [39]. η denotes the anisotropy parameter and is assumed to be zero for axially symmetric molecules [39]. Thus, under strong magnetic field, the total Hamiltonian of a quadrupolar nucleus partially oriented in liquid crystal matrix, having axial symmetric electric field gradient tensor, can be approximated as

$$H = \omega_o I_z + \frac{2\pi e^2 qQ}{[4I(2I-1)]}S(3I_z^2 - I^2) = \omega_o I_z + 2\pi\Lambda(3I_z^2 - I^2), \quad (2)$$

where $S = \langle(3\cos^2(\alpha)-1)/2\rangle$ is the order parameter at the site of the nucleus. If the order parameter S is small, the effective quadrupolar coupling Λ can be of the order of a few kHz in spite of e^2qQ being of the order of several MHz. Thus, it is possible to observe the satellite transitions due to first order quadrupolar coupling. A quadrupolar nucleus of spin I, having first order quadrupolar coupling, gives rise to 2I equi-spaced transitions [39,40]. If $(2I+1) = 2^n$, such a system can be treated as an n-qubit system [22,24]. The advantage of such systems and the dipolar coupled systems, over the J-coupled systems, is that the coupling values are one to two orders of magnitude larger, allowing shorter gate times or the use of shorter transition selective pulses [22–35]. It may be noted that, in quadrupolar and strongly dipolar coupled systems, implementation of single qubit gates, is not straight forward as in J-coupled systems, since the qubits are not individually addressed. However, in such systems single qubit gates are implemented by applying amplitude and phase modulated multi-frequency pulses [25], or by using strongly modulated pulses (SMPs) which are very robust and takes only few tens of microseconds [26,36–38]. Infact SMPs can extend the use of quadrupolar and dipolar coupled systems for implementing various quantum computing protocols [26,37,38]. So far quadrupolar systems have been used for, quantum simulation, preparation of pseudo pure states, implementation of quantum gates and search algorithms [25–34]. Recently Das et al. have implemented Cleve version of 2-qubit DJ algorithm on a spin-7/2 nucleus [35]. In all these cases the controlled gates are implemented by inverting populations between various levels, by using transition selective π pulses. Recently it has been demonstrated that non-adiabatic geometric phases can be used for implementing quantum gates [49,50]. Here we use non-adiabatic geometric phases to implement controlled phase shift gates and Collins version of DJ algorithm on a 3-qubit system obtained by eight eigen states of a spin-7/2 quadrupolar nucleus oriented in a liquid crystal medium.

A 50–50 mixture of cesium-pentadecafluoro-octanate and D_2O forms a lyotropic liquid crystal at room temperature [27]. The schematic energy level diagram of oriented spin-7/2 nucleus is shown in Fig. 1A. The eight energy levels are labeled as the basis states of a three qubit system. In the high field approximation, effective quadrupolar coupling (Λ) can be considered as a small perturbation to Zeeman field. Thus for population purposes the equilibrium density matrix can be considered to be proportional to H_z (Fig. 1A). Partially oriented ^{133}cesium nucleus (I = 7/2) gives rise to a well resolved seven transitions spectrum at room temperatures ranging from 290 to 315 K Fig. 1B. The effective quadrupolar coupling (Λ) changes with temperature, since the order parameter is a function of temperature. All the experiments have been carried out here at temperature 307 K, which gives $\Lambda = 6856$ Hz. The equilibrium spectrum is obtained by applying a $(\pi/2)_y$ pulse, is shown in Fig. 1B. The integrated intensities are in the expected ratio 7:12:15:16:15:12:7, as determined by the transition matrix elements of $|(I_{x(y)})_{ij}|^2$ [39,40]. Fluctuation of order parameter (S) leads to differential line broadening of the transitions, central transition is independent of orientation (or quadrupoalr coupling term H_Q^1) hence retains narrow line width [39,40].

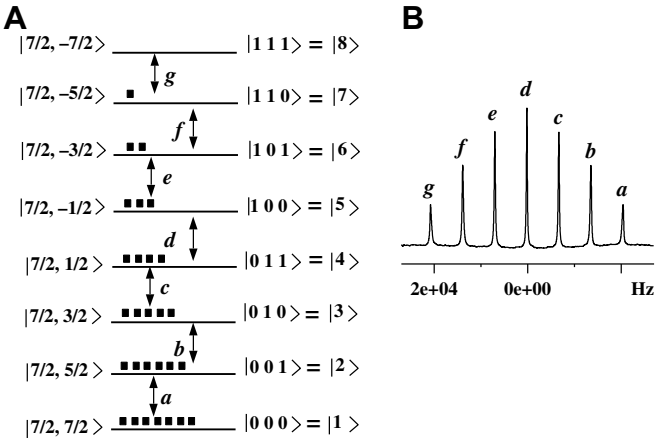

Fig. 1. (A) Schematic energy level diagram of a spin-7/2 nucleus, spin states $|7/2,7/2\rangle\cdots|7/2,-7/2\rangle$ are labeled as eight basis states of a three qubit system, the dark rectangles represent the equilibrium populations, and the single quantum transitions are labeled as a, b, …, g. (B) Equilibrium spectrum of oriented ^{133}Cs nucleus (spin-7/2), obtained by a non-selective $(\pi/2)_y$ pulse, at a resonance frequency of 65.59 MHz on a Bruker AV-500 spectrometer at a temperature 307 K. The distance between successive transitions is equal to the effective quadrupolar coupling (Λ). The line widths of transitions a, b, …, g are observed to be in the ratio 3.2:2.3:1.5:1.0:1.5:2.2:3.1 and the integrated experimental intensities are in the ratio 7.2:12.1:15.1:16:15.1:12.0:7.0 (theoretically expected 7:12:15:16:15:12:7).

2. Non-adiabatic geometric phases and controlled phase shift gates

Berry's discovery of geometric phase accompanying cyclic adiabatic evolution has triggered an immense effects in holonomy effects in quantum mechanics and has led to many generalizations [41]. The adiabatic theorem states that if a quantum system with a time-dependent non-degenerate Hamiltonian $H(t)$ is initially in nth instantaneous eigenstate of $H(0)$, and if $H(t)$ evolves slowly enough, then the state of the system at time 't' will remain in the nth instantaneous eigenstate of $H(t)$ [42]. Berry showed that, when a quantum system is parallel transported adiabatically round a circuit by varying parameters in its Hamiltonian, then it acquires a geometric phase factor in addition to the familiar dynamical phase factor [41]. Simon explained that this geometric phase could be viewed as a consequence of parallel transport in a curved space appropriate to the quantum system [42]. Aharonov and Anandan demonstrated that adiabatic condition can be lifted for cyclic evolution, and the resulting phase is known as non-adiabatic geometric phase or Aharonov and Anandan phase [43].

In nuclear magnetic resonance, geometric phase was first verified by Suter et al. [44], in the adiabatic regime. A similar approach was used by Jones, to implement controlled phase shift gates by geometric phases in a two qubit system formed by a weak J-coupling [45]. However the adiabatic condition is not satisfied in many realistic cases because of the long operation time [46]. Hence it is difficult to experimentally realize quantum computation with adiabatic evolutions, particularly for systems having short decoherence time [46]. To overcome this disadvantage, it was proposed

to use the non-adiabatic cyclic geometric phase to construct quantum gates [46,47]. For a non-adiabatic cyclic evolution, the total phase difference between the initial and final states, consists of both geometric and dynamical phases [43,46]. Therefore, to obtain only the non-adiabatic geometric phase, one has to remove the dynamical component. Non-adiabatic geometric phase in NMR was also first verified by Suter et al. [48]. Non-adiabatic geometric phases in NMR, were used to implement controlled phase shift gates, Deutsch–Jozsa (DJ) and Grover search algorithms in weakly J-coupled and strongly dipolar coupled systems [49,50]. In the following we show that, non-adiabatic geometric phases can be obtained by rotating a two level subspace, by means of transition selective pulses [48–50].

A two level subspace (r,s) forms a fictitious spin-1/2 subspace, hence the states $|r\rangle$ and $|s\rangle$ can be considered as basis states of a spin-1/2 nucleus, and can be represented on a Bloch sphere (Fig. 2) [39,48,50]. The (r,s) subspace can be manipulated by applying a transition selective pulse on $|r\rangle - |s\rangle$ transition, the unitary operator of this pulse in the (r,s) subspace is same as that of a pulse operator associated with spin-1/2 nucleus. In other words, the unitary operator of a transition selective pulse (TSP) with angle α and phase ϕ, is given by

$$U_{\mathrm{TSP}} = \mathrm{e}^{-\mathrm{i}\alpha(I_x^{rs}\cos(\phi)+I_y^{rs}\sin(\phi))} = \begin{pmatrix} \cos\alpha/2 & -\mathrm{e}^{-\mathrm{i}(\phi-\pi/2)}\sin\alpha/2 \\ \mathrm{e}^{(\mathrm{i}\phi-\pi/2)}\sin\alpha/2 & \cos\alpha/2 \end{pmatrix} \tag{3}$$

where $I_x^{rs} = I_x$ and $I_y^{rs} = I_y$ are the angular momentum operators of the (r,s) subspace. One can cyclically rotate the (r,s) subspace by applying two π pulses on transition (r,s), with phases (θ) and $(\theta+\pi+\phi)$ (Fig. 2), the resultant unitary operator, in the (r,s) subspace, is given by

$$\begin{aligned} u &= \mathrm{e}^{-\mathrm{i}\alpha(I_x^{rs}\cos(\theta)+I_y^{rs}\sin(\theta))}\cdot\mathrm{e}^{-\mathrm{i}\alpha(I_x^{rs}\cos(\theta+\pi+\phi)+I_y^{rs}\sin(\theta+\pi+\phi))} \\ &= \begin{pmatrix} 0 & -\mathrm{e}^{-\mathrm{i}(\theta-\pi/2)} \\ \mathrm{e}^{(\mathrm{i}\theta-\pi/2)} & 0 \end{pmatrix}\cdot\begin{pmatrix} 0 & -\mathrm{e}^{-\mathrm{i}(\theta+\phi+\pi/2)} \\ \mathrm{e}^{\mathrm{i}(\theta+\phi+\pi/2)} & 0 \end{pmatrix} \\ &= \begin{pmatrix} \mathrm{e}^{\mathrm{i}\phi} & 0 \\ 0 & \mathrm{e}^{-\mathrm{i}\phi} \end{pmatrix} \end{aligned} \tag{4}$$

Let $|r\rangle$ and $|s\rangle$, respectively represent lower and upper states of (r,s) subspace, then the effect of u on (r,s) subspace can be written as

$$\begin{aligned} u\,|r\rangle &= u\cdot\begin{pmatrix}1\\0\end{pmatrix} = \mathrm{e}^{\mathrm{i}\phi}\,|r\rangle \\ u\,|s\rangle &= u\cdot\begin{pmatrix}0\\1\end{pmatrix} = \mathrm{e}^{-\mathrm{i}\phi}\,|s\rangle \end{aligned} \tag{5}$$

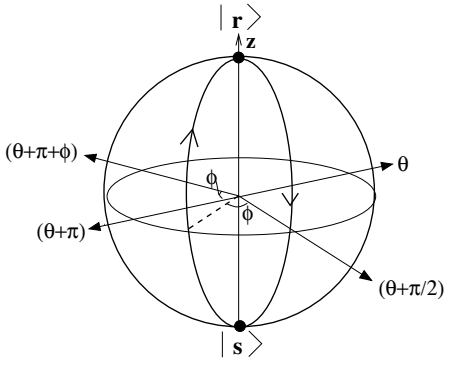

Fig. 2. A two level subspace (r,s) is represented on a Bloch sphere. Two π pulses applied on a transition (r,s) with phases θ and $(\theta+\pi+\phi)$, cyclically rotates the states $|r\rangle$ and $|s\rangle$. Solid angle subtended by this closed loop at the center of the sphere is, 2ϕ. The phase acquired by the states $|r\rangle$ and $|s\rangle$ is $\mathrm{e}^{\mathrm{i}\phi}$ and $\mathrm{e}^{-\mathrm{i}\phi}$, respectively.

Thus two π pulses applied on a transition (r,s), cyclically rotates each of the two states, and introduces phase factors $\mathrm{e}^{\mathrm{i}\phi}$ and $\mathrm{e}^{-\mathrm{i}\phi}$ respectively for $|r\rangle$ and $|s\rangle$ [48–50], where ϕ is half of the solid angle (Ω) of the cyclic path at the center of the Bloch sphere (Fig. 2), $\phi = \Omega/2$. Thus the phase, known as geometric phase, acquired by the states $|r\rangle$ and $|s\rangle$ is given by $\mathrm{e}^{\mathrm{i}\Omega/2}$ and $\mathrm{e}^{-\mathrm{i}\Omega/2}$, respectively [49,50], where the phase difference of $\mathrm{e}^{\mathrm{i}\pi}$ between the states indicate that the two states are traversed in the opposite directions [48,49]:

$$\begin{aligned} u\,|r\rangle &= \mathrm{e}^{\mathrm{i}\Omega/2}\,|r\rangle \\ u\,|s\rangle &= \mathrm{e}^{-\mathrm{i}\Omega/2}\,|s\rangle \end{aligned} \tag{6}$$

It is possible to obtain various solid angles, hence various geometric phases, by shifting the phases of the two π pulses with respect to each other (Fig. 2) [49,50].

However the internal Hamiltonian evolves during the application of the selective pulses, and gives rise to an additional phase known as dynamical phase. In order to observe only the geometric phase, one has to refocus the evolution of internal Hamiltonian. As shown in Eq. (2), the Hamiltonian consists of a Larmor frequency term and a quadrupolar coupling term. The Larmor frequency is identical to the frequency of central transition '*d*'. The transmitter and receiver frequencies are set at frequency of transition '*d*' (Fig. 1A), hence there is no evolution in the rotating frame due to the Larmor frequency term. Thus the evolution of internal Hamiltonian, during the pulse of duration t_p is a diagonal matrix, given by

$$\begin{aligned} U_{\mathrm{H}} = \mathrm{e}^{-\mathrm{i}H_{\mathrm{Q}}t_{\mathrm{p}}} = \mathrm{diag}[&\mathrm{e}^{i2\pi\Lambda 21t_{\mathrm{p}}}, \mathrm{e}^{\mathrm{i}2\pi\Lambda 3t_{\mathrm{p}}}, \mathrm{e}^{-\mathrm{i}2\pi\Lambda 9t_{\mathrm{p}}}, \mathrm{e}^{-\mathrm{i}2\pi\Lambda 15t_{\mathrm{p}}}, \mathrm{e}^{-\mathrm{i}2\pi\Lambda 15t_{\mathrm{p}}}, \\ &\mathrm{e}^{-\mathrm{i}2\pi\Lambda 9t_{\mathrm{p}}}, \mathrm{e}^{\mathrm{i}2\pi\Lambda 3t_{\mathrm{p}}}, \mathrm{e}^{\mathrm{i}2\pi\Lambda 21t_{\mathrm{p}}}] \end{aligned} \tag{7}$$

From Eq. (7), it is evident that the quadrupolar evolution can be refocused by choosing the value of t_p as $t_p = n/\Lambda$, where '*n*' is an integer. The selective pulses and multi-frequency pulses used in this work, are obtained by suitably phase modulating the on-resonance Gaussian pulse with 5000 digitized points. The duration of the pulse is chosen as 1.425 ms $(\approx 1/\Lambda)$.

The phase information can be encoded in the coherences, hence in order to observe the phases the initial state should contain the coherences, which is obtained by applying a non-selective $(\pi/2)_y$ pulse on equilibrium state. Fig. 3a shows the implementation of controlled phase shift gate, represented by the diagonal matrix $U^{\pi}_{(3,4)} = \mathrm{diag}[1,1,-1,-1,1,1,1,1]$, obtained by applying two selective π pulses on transition (3,4), with phases y and $(y+\pi+\pi) = y$. The two states $|0\,1\,0\rangle$ and $|0\,1\,1\rangle$ acquire π phase shift so the transitions 'b' and 'd' are inverted, confirming the phase gate. since the phases of two π pulses are same, it is possible to combine the two π pulses in to a single 2π pulse. Such pulses are used in Section 3.1.

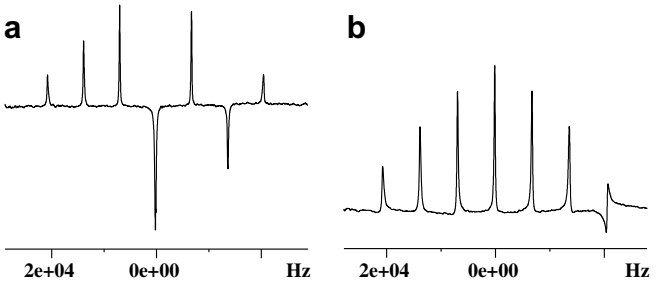

Fig. 3. Implementation of controlled phase shift gates (a) $U^{\pi}_{(3,4)} = \mathrm{diag}[1,1,-1,-1,1,1,1,1]$ and (b) $U_1^{\pi/2} = \mathrm{diag}[\mathrm{e}^{\mathrm{i}\pi/2},1,1,1,1,1,1,1]$, preceded by a hard $(\pi/2)_y$ pulse. $U^{\pi}_{(3,4)}$ is implemented by applying two $(\pi)_y$ pulses on transition *c*. $U_1^{\pi/2}$ is implemented by applying four multi-frequency π pulses (Eq. (10)).

In some quantum computing protocols (for example Grover search algorithm and quantum Fourier transform) one requires a phase gate such as U_k^{ϕ} (Table 1), which creates the relative phase $e^{i\phi}$ at kth state, for example $U_8^{\phi} = [1,1,1,1,1,1,1,e^{i\phi}]$. Such phase gates can be implemented by sandwiching various phase gates $u_{(i,j)}^{\phi}$, as shown in Table 1. $u_{(i,j)}^{\phi}$ indicates the geometric phase shift gate obtained by applying a pair of selective π pulses on a transition (i,j) with phases y and $(y+\pi+\phi)$, thus the diagonal elements corresponding to i and j states acquire a phase shift $e^{i\phi}$ and $e^{-i\phi}$ respectively. For example, $u_{(1,2)}^{\phi/8} = \mathrm{diag}[e^{i\phi/8}, e^{-i\phi/8}, 1,1,1,1,1,1]$, which can be obtained by applying two selective π pulse on transition (1,2) with phases y and $(y+\pi+\phi/8)$.

The method of constructing controlled phase shift gates (Table 1), is explained here. For example, consider a system consisting of N energy levels and $(N-1)$ single quantum transitions between the levels (1, 2), (2, 3), $\ldots(N-1,N)$, as shown in Fig. 4. In this system, the controlled phase shift gate $U_k^{\phi} = \mathrm{diag}[1_1, 1_2, \ldots, (e^{i\phi})_k, \ldots, 1_N]$, can be implemented by sandwiching $(N-1)$ phase shift gates, as

$$\begin{aligned} U_k^{\phi} &= u_{(1,2)}^{-\phi/N} u_{(2,3)}^{-2\phi/N} \cdot ------ \cdot\ u_{(k-1,k)}^{-(k-1)\phi/N} \cdot u_{(k,k+1)}^{(N-k)\cdot\phi/N} \\ &\quad \cdot u_{(k+1,k+2)}^{(N-(k+1))\cdot\phi/N} \cdot ------- \cdot\ u_{(N-1,N)}^{\phi/N} \\ &= (e^{-i\phi/N}) \cdot \mathrm{diag}[1_1, 1_2, \ldots, (e^{i\phi})_k, \ldots, 1_N] \end{aligned} \tag{8}$$

In Eq. (8) the overall (or) global phase factor $e^{-i\phi/N}$, has no physical significance since global phase is not an NMR observable quantity [39]. In NMR, each transition corresponding to a pair of eigen states, reflects the phase difference between those states. If all the states have a common phase factor then it will not be reflected in the spectrum. Hence in NMR quantum computing, the unitary operators which differ by an overall phase factor, are considered to be identical [14].

In Eq. (8), by putting $N = 8$ one can obtain any of the U_k^{ϕ} shown in Table 1. In Table 1, each of the operators, U_k^{ϕ}, requires seven pairs of selective π pulses, where each pair of pulses will act on a single transition. However the π pulses on unconnected transitions can be applied simultaneously. Hence one can simultaneously implement $u_{(1,2)}, u_{(3,4)}, u_{(5,6)}, u_{(7,8)}$ by using a pair of multi-frequency (MF) pulses, similarly $u_{(2,3)}, u_{(4,5)}, u_{(6,7)}$ can be implemented by using another pair of multi-frequency pulses. For example U_1^{ϕ} can be implemented by using seven geometric phase shift gates (Table 1), obtained by using two pairs of multi-frequency π pulses, as described below:

$$U_1^{\phi} = u_{(1,2)}^{7\phi/8} \cdot u_{(2,3)}^{3\phi/4} \cdot u_{(3,4)}^{5\phi/8} \cdot u_{(4,5)}^{\phi/2} \cdot u_{(5,6)}^{3\phi/8} \cdot u_{(6,7)}^{\phi/4} \cdot u_{(7,8)}^{\phi/8} \tag{9}$$

The unitary operators of phase shift gates correspond to diagonal matrices which commute with each other, hence U_1^{ϕ} of Eq. (9) can be rewritten as

$$\begin{aligned} U_1^{\phi} &= \left\{ \left[u_{(1,2)}^{7\phi/8}\right] \cdot \left[u_{(3,4)}^{5\phi/8}\right] \cdot \left[u_{(5,6)}^{3\phi/8}\right] \cdot \left[u_{(7,8)}^{\phi/8}\right] \right\} \\ &\quad \cdot \left\{ \left[u_{(2,3)}^{3\phi/4}\right] \cdot \left[u_{(4,5)}^{\phi/2}\right] \cdot \left[u_{(6,7)}^{\phi/4}\right] \right\} \\ &= \left\{ \left[(\pi)_y^a (\pi)_{y+\pi+7\phi/8}^a\right] \cdot \left[(\pi)_y^c (\pi)_{y+\pi+5\phi/8}^c\right] \cdot \left[(\pi)_y^e (\pi)_{y+\pi+3\phi/8}^e\right] \right. \\ &\quad \left. \cdot \left[(\pi)_y^g (\pi)_{y+\pi+\phi/8}^g\right] \right\} \\ &\quad \cdot \left\{ \left[(\pi)_y^b (\pi)_{y+\pi+3\phi/4}^b\right] \cdot \left[(\pi)_y^d (\pi)_{y+\pi+\phi/2}^d\right] \cdot \left[(\pi)_y^f (\pi)_{y+\pi+\phi/4}^f\right] \right\} \\ &= \left\{ \left[(\pi)_y^{a,c,e,g} \cdot (\pi)_{(y+\pi+7\phi/8),(y+\pi+5\phi/8),(y+\pi+3\phi/8),(y+\pi+\phi/8)}^{a,c,e,g}\right] \right\} \\ &\quad \cdot \left\{ \left[(\pi)_y^{b,d,f} \cdot (\pi)_{(y+\pi+3\phi/4),(y+\pi+\phi/2),(y+\pi+\phi/4)}^{b,d,f}\right] \right\} \end{aligned} \tag{10}$$

The π pulses acting on unconnected transitions, a, c, e and g (Eq. (10)), can be combined (added) in to a single pulse, since the operators of the subspaces corresponding to these transitions $I_{x(y)}^{(1,2)}, I_{x(y)}^{(3,4)}, I_{x(y)}^{(5.6)}$ and $I_{x(y)}^{(7,8)}$ [39,50], commute with each other. Similarly one can combine the (π) pulses acting unconnected transitions b, d and f (Eq. (10)). Fig. 3b shows the spectrum obtained by a $(\pi/2)_y$ pulse followed by the implementation of $U_1^{\phi}(\phi = \pi/2)$ using four MF-π pulses (Eq. (10)), the state $|000\rangle$ hence the transition 'a' acquires a $\pi/2$ phase shift, confirms $U_1^{\pi/2}$.

Table 1
Unitary operators of controlled-ϕ phase shifted gates with an overall phase factor $e^{-i\phi/8}$

$U_k^{\phi}(k = 1,2,\ldots,8)$
$U_1^{\phi} = \mathrm{diag}[e^{i\phi},1,1,1,1,1,1,1] = u_{(1,2)}^{7\phi/8} \cdot u_{(2,3)}^{3\phi/4} \cdot u_{(3,4)}^{5\phi/8} \cdot u_{(4,5)}^{\phi/2} \cdot u_{(5,6)}^{3\phi/8} \cdot u_{(6,7)}^{\phi/4} \cdot u_{(7,8)}^{\phi/8}$
$U_2^{\phi} = \mathrm{diag}[1,e^{i\phi},1,1,1,1,1,1] = u_{(1,2)}^{-\phi/8} \cdot u_{(2,3)}^{3\phi/4} \cdot u_{(3,4)}^{5\phi/8} \cdot u_{(4,5)}^{\phi/2} \cdot u_{(5,6)}^{3\phi/8} \cdot u_{(6,7)}^{\phi/4} \cdot u_{(7,8)}^{\phi/8}$
$U_3^{\phi} = \mathrm{diag}[1,1,e^{i\phi},1,1,1,1,1] = u_{(1,2)}^{-\phi/8} \cdot u_{(2,3)}^{-\phi/4} \cdot u_{(3,4)}^{5\phi/8} \cdot u_{(4,5)}^{\phi/2} \cdot u_{(5,6)}^{3\phi/8} \cdot u_{(6,7)}^{\phi/4} \cdot u_{(7,8)}^{\phi/8}$
$U_4^{\phi} = \mathrm{diag}[1,1,1,e^{i\phi},1,1,1,1] = u_{(1,2)}^{-\phi/8} \cdot u_{(2,3)}^{-\phi/4} \cdot u_{(3,4)}^{-3\phi/8} \cdot u_{(4,5)}^{\phi/2} \cdot u_{(5,6)}^{3\phi/8} \cdot u_{(6,7)}^{\phi/4} \cdot u_{(7,8)}^{\phi/8}$
$U_5^{\phi} = \mathrm{diag}[1,1,1,1,e^{i\phi},1,1,1] = u_{(1,2)}^{-\phi/8} \cdot u_{(2,3)}^{-\phi/4} \cdot u_{(3,4)}^{-3\phi/8} \cdot u_{(4,5)}^{\phi/2} \cdot u_{(5,6)}^{3\phi/8} \cdot u_{(6,7)}^{\phi/4} \cdot u_{(7,8)}^{\phi/8}$
$U_6^{\phi} = \mathrm{diag}[1,1,1,1,1,e^{i\phi},1,1] = u_{(1,2)}^{-\phi/8} \cdot u_{(2,3)}^{-\phi/4} \cdot u_{(3,4)}^{-3\phi/8} \cdot u_{(4,5)}^{-\phi/4} \cdot u_{(5,6)}^{-5\phi/8} \cdot u_{(6,7)}^{\phi/4} \cdot u_{(7,8)}^{\phi/8}$
$U_7^{\phi} = \mathrm{diag}[1,1,1,1,1,1,e^{i\phi},1] = u_{(1,2)}^{-\phi/8} \cdot u_{(2,3)}^{-\phi/4} \cdot u_{(3,4)}^{-3\phi/8} \cdot u_{(4,5)}^{-\phi/2} \cdot u_{(5,6)}^{-5\phi/8} \cdot u_{(6,7)}^{-6\phi/8} \cdot u_{(7,8)}^{\phi/8}$
$U_8^{\phi} = \mathrm{diag}[1,1,1,1,1,1,1,e^{i\phi}] = u_{(1,2)}^{-\phi/8} \cdot u_{(2,3)}^{-\phi/4} \cdot u_{(3,4)}^{-3\phi/8} \cdot u_{(4,5)}^{-\phi/2} \cdot u_{(5,6)}^{-5\phi/8} \cdot u_{(6,7)}^{-3\phi/4} \cdot u_{(7,8)}^{-7\phi/8}$

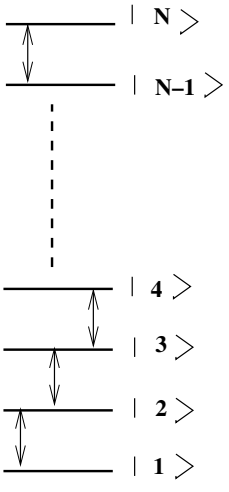

Fig. 4. Schematic energy level diagram of an N-level system. The arrows represent single quantum transitions.

3. Collins version of DJ algorithm

An n-bit binary string (x) has 2^n possible input states, $x = (000\cdots0)_n, \ldots, (111\cdots1)_n$. Consider a function '$f$' which takes '$n$' input bits and returns one output bit, that is $f(x) = 0$ or 1. Further more, it is told that the function 'f' is either constant or balanced; when 'f' is constant, $f(x) = 0$ or 1 for all the input states, whereas if 'f'is balanced then $f(x) = 0$ for half of the input states and $f(x) = 1$ for the remaining half. Classically one has to evaluate $f(x)$ for each of the input states separately. As soon as function returns '0' for some inputs and '1' for other inputs, it is certainly a balanced function. However, if the output is still the same after trying $2^n/2$ different input states, the function 'f' might be still balanced, even though most likely it is constant. Only when $(2^n/2+1)$ input states produce the same output, you can be sure that 'f' is balanced. Thus in the worst case, one requires $(2^n/2+1)$ queries [6].

On the other hand, the Deutsch–Jozsa (DJ) algorithm can evaluate the function, simultaneously for all 2^n input states and thus it requires only one query to determine the nature of the function

[3,6,51]. The Cleve version of the DJ algorithm requires an extra qubit, thus for an n-bit function one requires $(n+1)$ qubit system with initial state, $\psi_{in} = |\, 0_1 0_2 \cdots 0_n\rangle \,|\, 1_{n+1}\rangle$. The algorithm consists of four steps [6,51];(1) creation of superposition state of all the input states by applying Hadamard gates on all the qubits, (2) implementation of the oracle, (3) converting the resultant state in to one of the basis states with Hadamard gate on first n qubits [51], (4) measurement of final state of first 'n' qubits. For constant function, the final state of each of the n qubits is $|\, 0\rangle$, whereas for balanced function, atleast one of the 'n' qubits is in state $|\, 1\rangle$. The first and third steps require Hadamard gates, whereas the second step, implementation of oracle, require controlled not gates. Collins version of DJ algorithm is same as Cleave's version, except that it uses only 'n' input qubits for an n-bit function, and oracle requires controlled phase shift gates [52].

In NMR the final state of this algorithm (both Cleave and Collins version) corresponds to longitudinal magnetization (populations), hence qubit selective $(\pi/2)_y$ pulses are required for the measurement, these pulses cancel the $(\pi/2)_{-y}$ pulses required for the second set of Hadamard gates (step 3). It was showed that the phase sensitive spectrum recorded immediately after the oracle implementation, can distinguish constant and balanced functions [11,31,35]. Thus the implementation of DJ algorithm on an NMR QC, can be simplified to the following steps: (1) creation of superposition state of all the input states, (2) implementation of the oracle, (3) detection. In this approach, the final state corresponds to a coherent superposition of all the basis states, and the phase sensitive detection of single quantum coherences can reveal the nature of the function that is encoded in the oracle operator.

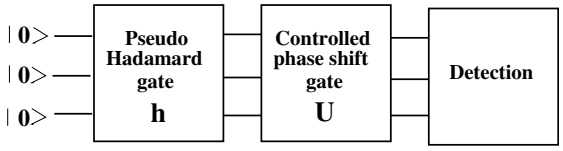

Fig. 5. Quantum circuit for Collins version of DJ algorithm on a three qubit system.

For a three qubit system there are 2 constant and 70 $(c^N_{N/2} = c^8_4)$ balanced functions [52,53]. The quantum circuit of the Collins version of the DJ algorithm is shown in Fig. 5. The algorithm starts with a pure state (pseudo pure state in NMR) $|\, 000\rangle$ which is converted to a superposition state of eight basis states $|\, 000\rangle, |\, 001\rangle, \ldots, |\, 111\rangle$, by applying a pseudo Hadamard gate on all the three qubits. Thereafter a unitary operator U (oracle) is applied, followed by detection. The unitary operators (U) of the oracle, are eight dimensional diagonal matrices. For two constant functions, U's are given by

$$\begin{aligned} &U_{c1} = I \text{ (unit matrix) and} \\ &U_{c2} = \mathrm{diag}[-1,-1,-1,-1,-1,-1,-1,-1] = (-1)\cdot I \end{aligned} \tag{11}$$

For balanced functions, we define the unitary operator as $U(1,k,l,m)$, which means that each of the four diagonal elements $1, k, l$, and m are equal to $e^{i\pi}$ or $e^{-i\pi}$ (=−1), whereas the remaining four diagonal elements are 1. For example $U(1,2,3,4) = \mathrm{diag}[-1,-1,-1,-1,1,1,1,1]$. The unitary operators of 35 balanced functions can be written as

$$\begin{aligned} &U(1,k,l,m) = [-\,|\,1\rangle\langle 1\,|\,- \,|\,k\rangle\langle k\,|\,- \,|\,l\rangle\langle l\,|\,- \,|\,m\rangle\langle m\,|]\cdot I, \\ &\text{where} \quad k < l < m, k = 2,3,\ldots,6, l \geqslant k+1, \text{ and } m \geqslant l+1 \end{aligned} \tag{12}$$

The unitary operators of the remaining 35 balanced functions are identical to one of the operators of Eq. (12), up to an overall phase factor $e^{i\pi}$ [53]. Here we implement the unitary operators corresponding to 11 of the 35 balanced functions (Eq. (12)) and one constant function (U_{c1}).

3.1. Experimental implementation

3.1.1. Preparation of pseudo pure state (PPS) $|\, 000\rangle$

A multi-frequency pulse with six harmonics with appropriate amplitudes was applied. The six harmonics are the frequencies of the six leftmost transitions $b, c, \ldots, g$ of Fig. 1B. Under the influence of this pulse, the populations of all the states except $|\, 000\rangle$, start a collective population transfer among them as a linear chain of cou-

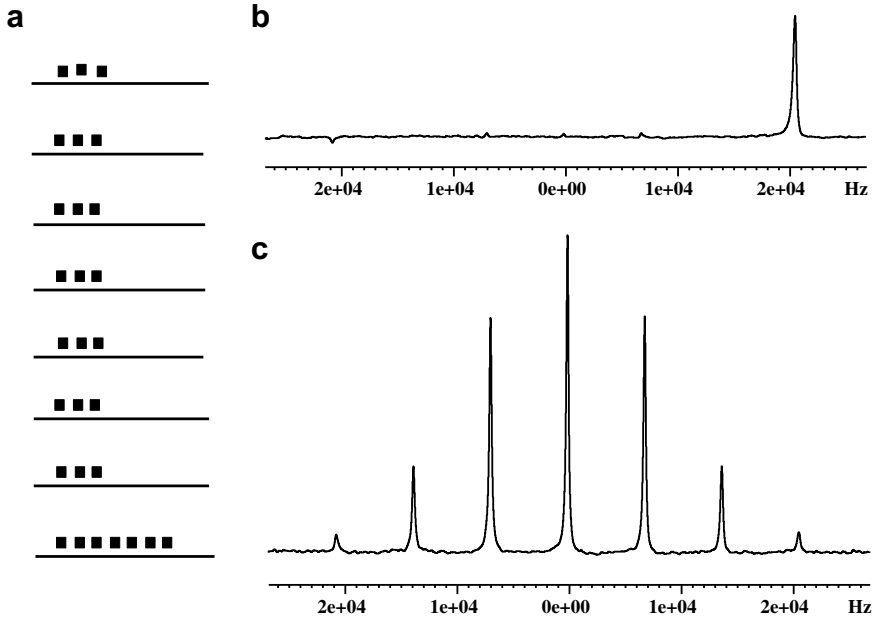

Fig. 6. (a) Population distribution of $|\, 000\rangle$ PPS obtained by applying an amplitude modulated multi-frequency pulse (explained in text) on transitions b, c, d, e, f, and g at equilibrium state. (b) Spectrum of $|\, 000\rangle$ PPS obtained by applying a non-selective 5° pulse with 32 scans. (c) Coherent superposition state (Eqs. (13) and (14)) obtained by applying a $(\pi/2)_y$ pulse on $|\, 000\rangle$ PPS. The intensities are in accordance with Eq. (13), which is different from equilibrium intensities of Fig. 1. Experimental integrated intensities are in the ratio 10:48:101:140:100:46:8, while the expected theoretical intensities are in the ratio 7:42:105:140:105:42:7. The intensities here represent unequal superposition of basis states.

pled oscillators [8,14,27]. Choosing the correct amplitudes of various harmonics and duration of the pulse, these six transitions can be simultaneously saturated with average population of these seven levels. The relative amplitudes of the six harmonics *b*, *c*, ..., and *g* are respectively given by 0.84, 0.93, 1, 1.03, 1.04 and 1.07 [35]. The duration of the pulse is 2.05 ms. A gradient pulse was applied subsequently to kill (dephase) the coherences created during the process. The final populations were measured using a non-selective small-angle (5°) pulse. The small-angle pulse, converts the population differences between adjacent energy levels into single quantum transitions, within linear approximation. The spectrum of Fig. 6b confirms the preparation of $|000\rangle$ pseudopure state.

3.1.2. Coherent superposition

After the creation of $|000\rangle$ PPS, a pseudo Hadamard gate (h) has to be applied for creating a superposition of 8 basis states. In weakly coupled spins-1/2 nuclei, '*h*' is implemented by a hard $(\pi/2)_y$ pulse which creates an equal superposition. In the present case the hard $(\pi/2)_y$ pulse creates an unequal superposition state, since the coefficients of various eigenstates are different. In other words, the unitary operator of a hard $(\pi/2)_y$ is not same as that of a weekly coupled three qubit system. However, as is shown here, the created coherent superposition can be utilized for quantum parallelism, to distinguish different classes of functions. The state of the system after a $(\pi/2)_y$ pulse on $|000\rangle$ PPS, is given by

$$\begin{aligned}|\psi\rangle = (e^{-i\frac{\pi}{2}I_y})\cdot|000\rangle &= \frac{1}{8\sqrt{2}}[|000\rangle + \sqrt{7}\,|001\rangle + \sqrt{21}\,|010\rangle \\ &+ \sqrt{35}\,|011\rangle + \sqrt{35}\,|100\rangle + \sqrt{21}\,|101\rangle + \sqrt{7}\,|110\rangle \\ &+ |111\rangle] = \frac{1}{8\sqrt{2}}[|1\rangle + \sqrt{7}\,|2\rangle + \sqrt{21}\,|3\rangle + \sqrt{35}\,|4\rangle \\ &+ \sqrt{35}\,|5\rangle + \sqrt{21}\,|6\rangle + \sqrt{7}\,|7\rangle + |8\rangle] \end{aligned} \tag{13}$$

The corresponding density matrix can be written as

$$\sigma = |\psi\rangle\langle\psi| = \frac{1}{128}\cdot \begin{array}{c} \begin{matrix} |1\rangle & |2\rangle & |3\rangle & |4\rangle & |5\rangle & |6\rangle & |7\rangle & |8\rangle \end{matrix} \\ \begin{pmatrix} 1 & \boxed{\sqrt{7}} & \sqrt{21} & \sqrt{35} & \sqrt{35} & \sqrt{21} & \sqrt{7} & 1 \\ \boxed{\sqrt{7}} & 7 & \boxed{\sqrt{147}} & \sqrt{245} & \sqrt{245} & \sqrt{147} & 7 & \sqrt{7} \\ \sqrt{21} & \boxed{\sqrt{147}} & 21 & \boxed{\sqrt{735}} & \sqrt{735} & 21 & \sqrt{147} & \sqrt{21} \\ \sqrt{35} & \sqrt{245} & \boxed{\sqrt{735}} & 35 & \boxed{35} & \sqrt{245} & \sqrt{147} & \sqrt{35} \\ \sqrt{35} & \sqrt{245} & \sqrt{735} & \boxed{35} & 35 & \boxed{\sqrt{735}} & \sqrt{147} & \sqrt{35} \\ \sqrt{21} & \sqrt{147} & 21 & \sqrt{735} & \boxed{\sqrt{735}} & 21 & \boxed{\sqrt{147}} & \sqrt{21} \\ \sqrt{7} & 7 & \sqrt{147} & \sqrt{245} & \sqrt{245} & \boxed{\sqrt{147}} & 7 & \boxed{\sqrt{7}} \\ 1 & \sqrt{7} & \sqrt{21} & \sqrt{35} & \sqrt{35} & \sqrt{21} & \boxed{\sqrt{7}} & 1 \end{pmatrix} \begin{matrix} |1\rangle \\ |2\rangle \\ |3\rangle \\ |4\rangle \\ |5\rangle \\ |6\rangle \\ |7\rangle \\ |8\rangle \end{matrix} \end{array} . \tag{14}$$

where the elements within the boxes represent single quantum transitions *a*, *b*, ..., *g*. Fig. 6c shows the spectrum of $|\psi\rangle$, where the intensities of transitions are obtained by modulus of the product of single quantum elements of Eq. (14), with corresponding matrix elements of I_x. The intensities in Fig. 6c are different from equilibrium intensities, and represent the coherent superposition of the basis states.

3.1.3. Implementation of U

For constant function $U = U_{c1} = I$ (unit matrix), which requires no pulse, thus the final state ψ_{c1} is given by

$$|\psi_{c1}\rangle = U_{c1}\,|\psi\rangle = |\psi\rangle \tag{15}$$

As mentioned in Section 2, the controlled phase shift gate $U^{\pi}_{(i,j)}$ can be achieved by applying two (π) pulses with same phase on transition (i,j), which can be combined in to a single (2π) pulse. For balance functions, $U = U(1,k,l,m)$ (Eq. (12)), can be decomposed in to

Table 2
Unitary operators of balanced functions (Eq. (12)) and corresponding pulse sequences, consisting of 2π pulses, where all the pulses are applied with phase '*y*'

$U(1,k,l,m)$	Pulse sequence
$U(1,2,3,4)$	$(2\pi)^{a,c}$
$U(1,2,3,7)$	$(2\pi)^{a,c,e}(2\pi)^{d,f}$
$U(1,2,4,6)$	$(2\pi)^{a,d}(2\pi)^{e}$
$U(1,2,5,6)$	$(2\pi)^{a,e}$
$U(1,2,6,7)$	$(2\pi)^{a,f}$
$U(1,3,4,5)$	$(2\pi)^{a,d}(2\pi)^{b}$
$U(1,3,4,8)$	$(2\pi)^{a,d,f}(2\pi)^{b,e,g}$
$U(1,3,5,8)$	$(2\pi)^{a,e,g}(2\pi)^{b,f}$
$U(1,3,7,8)$	$(2\pi)^{a,g}(2\pi)^{b}$
$U(1,4,5,8)$	$(2\pi)^{a,c,e,g}(2\pi)^{b,f}$
$U(1,4,7,8)$	$(2\pi)^{a,c,g}(2\pi)^{b}$
$U(1,5,7,8)$	$(2\pi)^{a,c,g}(2\pi)^{b,d}$
$U(1,2,3,5)$	$(2\pi)^{a,c}\ (2\pi)^{d}$
$U(1,2,3,8)$	$(2\pi)^{a,c,e,g}(2\pi)^{d,f}$
$U(1,2,4,7)$	$(2\pi)^{a,d,f}(2\pi)^{e}$
$U(1,2,5,7)$	$(2\pi)^{a,e}(2\pi)^{f}$
$U(1,2,6,8)$	$(2\pi)^{a,f}(2\pi)^{g}$
$U(1,3,4,6)$	$(2\pi)^{a,d}(2\pi)^{b,e}$
$U(1,3,5,6)$	$(2\pi)^{a,e}(2\pi)^{b}$
$U(1,3,6,7)$	$(2\pi)^{a,f}(2\pi)^{b}$
$U(1,4,5,6)$	$(2\pi)^{a,c,e}(2\pi)^{b}$
$U(1,4,6,7)$	$(2\pi)^{a,c,f}(2\pi)^{b}$
$U(1,5,6,7)$	$(2\pi)^{a,c,f}(2\pi)^{b,d}$
$U(1,6,7,8)$	$(2\pi)^{a,c,e,g}(2\pi)^{b,d}$
$U(1,2,3,6)$	$(2\pi)^{a,c,e}(2\pi)^{d}$
$U(1,2,4,5)$	$(2\pi)^{a,d}$
$U(1,2,4,8)$	$(2\pi)^{a,d,f}(2\pi)^{e,g}$
$U(1,2,5,8)$	$(2\pi)^{a,e,g}(2\pi)^{f}$
$U(1,2,7,8)$	$(2\pi)^{a,g}$
$U(1,3,4,7)$	$(2\pi)^{a,d,f}(2\pi)^{b,e}$
$U(1,3,5,7)$	$(2\pi)^{a,e}(2\pi)^{b,f}$
$U(1,3,6,8)$	$(2\pi)^{a,f}(2\pi)^{b,g}$
$U(1,4,5,7)$	$(2\pi)^{a,c,e}(2\pi)^{b,f}$
$U(1,4,6,8)$	$(2\pi)^{a,c,f}(2\pi)^{b,g}$
$U(1,5,6,8)$	$(2\pi)^{a,c,f}(2\pi)^{b,d,g}$

$$\begin{aligned} U(1,k,l,m) &= u^{\pi}_{(1,k)}\cdot u^{\pi}_{(l,m)} \\ &= [u^{\pi}_{(1,2)}\cdots u^{\pi}_{(k-1,k)}][u^{\pi}_{(l,l+1)}\cdot u^{\pi}_{(l+1,l+2)}\cdots u^{\pi}_{(m-1,m)}] \end{aligned} \tag{16}$$

In Eq. (16), $u^{\pi}_{(1,k)}$ and $u^{\pi}_{(l,m)}$ are implemented by applying two $(2\pi)_y$ pulses on transitions (1,k) and (l,m) respectively, if (1,k) and (l,m) does not correspond to single quantum transitions, then they can be decomposed in to a series of single quantum transitions, as shown in the second equality of Eq. (16), for example

$$\begin{aligned} U(1,2,3,4) &= u^{\pi}_{(1,2)}\cdot u^{\pi}_{(3,4)} = (2\pi)^{a}\cdot(2\pi)^{c} \\ U(1,4,5,8) &= u^{\pi}_{(1,4)}\cdot u^{\pi}_{(5,8)} = [u^{\pi}_{(1,2)}.u^{\pi}_{(2,3)}\cdot u^{\pi}_{(3,4)}].[u^{\pi}_{(5,6)}\cdot u^{\pi}_{(6,7)}\cdot u^{\pi}_{(7,8)}] \\ &= [(2\pi)^{a}\cdot(2\pi)^{b}\cdot(2\pi)^{c}]\cdot[(2\pi)^{e}\cdot(2\pi)^{f}\cdot(2\pi)^{g}] \\ &= (2\pi)^{a,c,e,g}\cdot(2\pi)^{b,f} \end{aligned} \tag{17}$$

where in the last equality of Eq. (17), the pulses acting on unconnected transitions (Fig. 1) are combined in to a single MF pulse. The required pulses for various $U(1,k,l,m)$ of Eq. (12) are given in Table 2, the 2π pulses acting on unconnected transitions, are combined in to a single multi-frequency (MF) 2π pulse. The duration of each transition selective pulse, is set such that the evolution due to quadrupolar coupling, makes a complete 2π rotation. It is to be noted that, in Eq. (17) and Table 2, one can use any phase for (2π) pulses, we have used '*y*' phase for all the pulses. The final state $|\psi_{1,k,l,m}\rangle$ is given by

$$|\psi_{1,k,l,m}\rangle = U(1,k,l,m)\,|\psi\rangle \tag{18}$$

It can be seen that $|\psi_{1,k,l,m}\rangle$ is same as $|\psi\rangle$, except that the basis states $|1\rangle$, $|k\rangle$, $|l\rangle$ and $|m\rangle$ acquire a phase factor $e^{i\pi}$ (=−1)

3.1.4. Detection

The single quantum transitions (*a*, *b*, *g*) of the final states (Eq. (15),(18)) are detected. Fig. 7 shows the spectrum of $|\psi_{c1}\rangle$ and various $|\psi_{1,k,l,m}\rangle$. From the shape of the spectrum one can conclude, whether the final state represents a constant (or) a balanced function. For constant function ($|\psi_{c1}\rangle$) none of the peaks are inverted, whereas for balanced functions ($|\psi_{1klm}\rangle$) atleast one of the peaks is inverted. Furthermore the phases of transitions confirm the final state $|\psi_{1,k,l,m}\rangle$. For example in the spectrum of $|\psi_{1,2,3,4}\rangle$, transition *d* is negative since the phase difference between the states $|4\rangle$ and $|5\rangle$ is $e^{i\pi}$, while all others have zero phase difference, similarly one can confirm the other states.

It is to be noted that, though the final state (Eq. (18)) contains single and multiple quantum coherences, the nature of the function encoded in the unitary operator (*U*) of the oracle, is determined by phase sensitive spectra of single quantum coherences. Thus for implementing DJ algorithm in NMR QC, it is sufficient to have the initial state containing only single quantum coherences, which can be obtained by applying a $(\pi/2)$ pulse on an equilibrium state [54]. Infact, it has been shown that, the thermal initial states are sufficient to implement some algorithms of interest [55–57]. However the implementation of DJ algorithm using coherent superposition state, demonstrate the coherent control of a

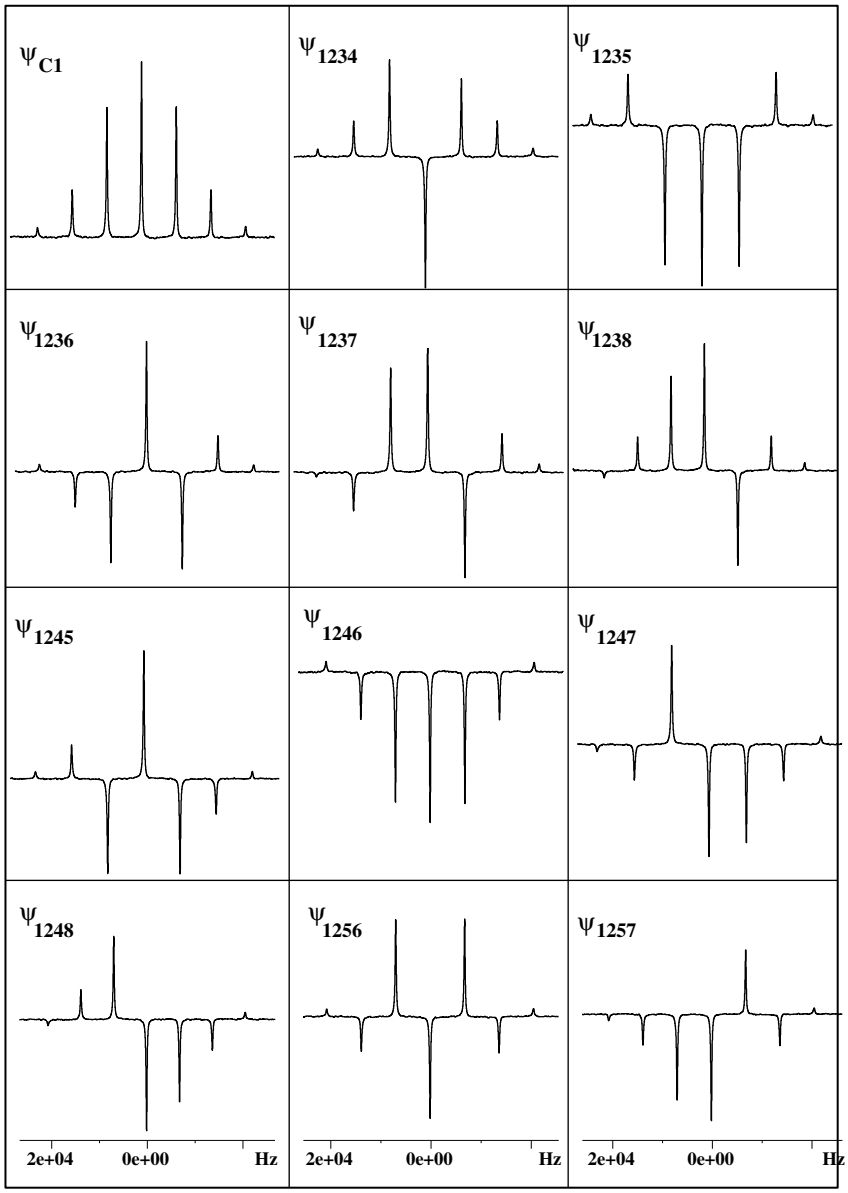

Fig. 7. Implementation of Collins version of 3-qubit DJ algorithm (Fig. 5). Spectrum of ψ_{c1} which corresponds to a constant function $U = I$. Spectra of $\psi_{1,k,l,m}$ (Eq. (18)) which correspond to balanced functions $U(1,k,l,m)$ (Eq. (12)). The required MF pulses for implementing $U(1,k,l,m)$ are given in Table 2. The duration of each MF pulse is 1.425 ms. Each spectrum is recorded in 4 scans.

superposition state, which will be helpful in extending the use of these systems for other quantum algorithms.

4. Conclusions

Demonstration of quantum computing protocols on various NMR systems, is a promising research area for increasing number of qubits. In this work controlled phase shift gates are implemented on a oriented spin-7/2 nucleus, using non-adiabatic geometric phases obtained by using selective pulses on single quantum transitions. It is also demonstrated here that in an N level system, one can implement a controlled phase shift gate by sandwiching various geometric phase shift gates, this method can also be applied to weakly as well as strongly coupled spin-1/2 systems. The number of selective pulses are reduced by using multi-frequency (MF) pulses. Collins version of 3-qubit DJ algorithm is implemented, where the eight basis states are collectively treated as a three qubit system. The required controlled phase shift gates of the algorithm, are implemented by using MF-(2π) pulses. Though it is difficult to scale the quadrupolar systems for higher number of qubits, the implementation of QIP on these systems, will be helpful in extending their applicability in larger spin networks where quadrupolar nuclei are coupled to spin-1/2 nuclei.

References

[1] P. Benioff, Quantum mechanical models of turing machines that dissipate no energy, Phys. Rev. Lett. 48 (1982) 1581.
[2] D. Deutsch, Quantum theory, the Church-Turing principle and the universal quantum computer, Proc. R. Soc. London, Ser. A 400 (1985) 97.
[3] D. Deutsch, R. Jozsa, Rapid solution of problems by quantum computation, Proc. R. Soc. Lond. A 439 (1992) 553.
[4] P.W. Shor, Polynominal-time algorithms for prime factorization and discrete algorithms on quantum computer, SIAM Rev. 41 (1999) 303–332.
[5] L.K. Grover, Quantum mechanics helps in searching for a needle in haystack, Phys. Rev. Lett. 79 (1997) 325.
[6] M.A. Nielsen, I.L. Chuang, Quantum Computation and Quantum Information, Cambridge University Press, Cambridge, UK, 2000.
[7] M. Scholz, T. Aichele, S. Ramelow, O. Benson, Deutsch–Jozsa algorithm using triggered single photons from a single quantum dot, Phys. Rev. Lett. 96 (2006) 180501.
[8] D.G. Cory, A.F. Fahmy, T.F. Havel, Ensemble quantum computing by NMR spectroscopy, Proc. Natl. Acad. Sci. USA 94 (1997) 1634.
[9] N. Gershenfield, I.L. Chuang, Bulk spin-resonance quantum computation, Science 275 (1997) 350.
[10] I.L. chuang, L.M.K. Vanderspyen, X. Zhou, D.W. Leung, S. Llyod, Experimental realization of a quantum algorithm, Nature (London) 393 (1998) 1443.
[11] J.A. Jones, M. Mosca, Implementation of a quantum algorithm on a nuclear magnetic resonance quantum computer, J. Chem. Phys. 109 (1998) 1648.
[12] I.L. Chuang, N. Gershenfeld, M. Kubinec, Experimental implementation of fast quantum searching, Phys. Rev. Lett. 80 (1998) 3408.
[13] T.S. Mahesh, K. Dorai, Arvind, A. Kumar, Implementing logic gates and the DeutschJozsa quantum algorithm by two-dimensional nmr using spin- and transition-selective pulses, J. Mag. Res. 148 (2001) 95.
[14] D.G. Cory, M.D. Price, T.F. Havel, An experimentally accessible paradigm for quantum computing, Physica D 120 (1998) 82.
[15] M.D. Price, S.S. Somaroo, C.H. Tseng, J.C. Gore, A.F. Fhamy, T.F. Havel, D.G. Cory, Construction and implementation of NMR quantum logic gates for two spin systems, J. Mag. Res. 140 (1999) 371.
[16] M.D. Price, S.S. Somaroo, A.E. Dunlop, T.F. Havel, D.G. Cory, Generalized methods for the development of quantum logic gates for an NMR quantum information processor, Phys. Rev. A 60 (1999) 2777.
[17] M.D. Price, T.F. Havel, D.G. Cory, Multiqubit logic gates in NMR quantum computing, New J. Phys. 2 (2000) 10.
[18] E. Farhi, J. Goldstone, S. Guttmann, J. Lapan, A. Lundgren, D. Preda, A quantum adiabatic evolution algorithm applied to random instances of an NP-complete problem, Science 292 (2001) 472.
[19] A.M. Childs, E. Farhi, J. Preskill, Robustness of adiabatic quantum computation, Phys. Rev. A 65 (2002) 012322.
[20] M. Steffen, W. van Dam, T. Hogg, G. Bryeta, I. Chuang, Experimental implementation of an adiabatic quantum optimization algorithm, Phys. Rev. Lett. 90 (2003) 067903.
[21] B.M. Fung, Use of pairs of pseudopure states for NMR quantum computing, Phys. Rev. A 63 (2001) 022304.
[22] A.K. Khitrin, B.M. Fung, Nuclear magnetic resonance quantum logic gates using quadrupolar nuclei, J. Chem. Phys. 112 (2000) 6963.
[23] T.S. Mahesh, N. Sinha, K.V. Ramanathan, A. Kumar, Ensemble quantum-information processing by NMR: implementation of gates and the creation of pseudopure states using dipolar coupled spins as qubits, Phys. Rev. A 65 (2002) 022312.
[24] N. Sinha, T.S. Mahesh, K.V. Ramanathan, A. Kumar, Toward quantum information processing by nuclear magnetic resonance: pseudopure states and logical operations using selective pulses on an oriented spin 3/2 nucleus, J. Chem. Phys. 114 (2001) 4415.
[25] V.L. Ermakov, B.M. Fung, Experimental realization of a continuous version of the Grover algorithm, Phys. Rev. A 66 (2002) 042310.
[26] H. Kampermann, W.S. Veeman, Characterization of quantum algorithms by quantum process tomography using quadrupolar spins in solid-state nuclear magnetic resonance, J. Chem. Phys. 122 (2005) 214108.
[27] A. Khitrin, H. Sun, B.M. Fung, Method of multifrequency excitation for creating pseudopure states for NMR quantum computing, Phys. Rev. A 63 (2001) 020301.
[28] A.K. Khitrin, B.M. Fung, NMR simulation of an eight-state quantum system, Phys. Rev. A 64 (2001) 032306.
[29] K.V.R.M. Murali, N. Sinha, T.S. Mahesh, M. Levitt, K.V. Ramanathan, A. Kumar, Quantum-information processing by nuclear magnetic resonance: experimental implementation of half-adder and subtractor operations using an oriented spin-7/2 system, Phys. Rev. A 66 (2002) 022313.
[30] A. Kumar, K.V. Ramanathan, T.S. Mahesh, N. Sinha, K.V.R.M. Murali, Developments in quantum information processing by NMT: Use of quadrupolar and dipolar couplings, Pramana J. Phys. 59 (2) (2002) 243–254.
[31] R. Das, A. Kumar, Use of quadrupolar nuclei for quantum-information processing by nuclear magnetic resonance: implementation of a quantum algorithm, Phys. Rev. A 68 (2003) 032304.
[32] R.S. Sarthour, E.R. deAzevedo, F.A. Bonk, E.L.G. Vidoto, T.J. Bonagamba, A.P. Guimaraes, J.C.C. Freitas, I.S. Oliveira, Relaxation of coherent states in a two-qubit NMR quadrupole system, Phys. Rev. A 68 (2003) 022311.
[33] F.A. Bonk, R.S. Sarthour, E.R. deAzevedo, J.D. Bulnes, G.L. Mantovani, J.C.C. Freitas, T.J. Bonagamba, A.P. Guimaraes, I.S. Oliveira, Quantum-state tomography for quadrupole nuclei and its application on a two-qubit system, Phys. Rev. A 69 (2004) 042322.
[34] F.A. Bonk, E.R. deAzevedo, R.S. Sarthour, J.D. Bulnes, J.C.C. Freitas, A.P. Guimaraes, I.S. Oliveira, T.J. Bonagamba, Quantum logical operations for spin 3/2 quadrupolar nuclei monitored by quantum state tomography, J. Magn. Res. 175 (2005) 226.
[35] R. Das, A. Kumar, Experimental implementation of a quantum algorithm in a multiqubit NMR system formed by an oriented spin-7/2 system, Appl. Phys. Lett. 89 (2006) 024107.
[36] E.M. Fortunato, M.A. Pravia, N. Boulant, G. Teklemariam, T.F. Havel, D.G. Cory, Strongly modulating pulses to implement precise effective Hamiltonian for quantum information processing, J. Chem. Phys. 116 (2002) 7599.
[37] T.S. Mahesh, D. Suter, Quantum-information processing using strongly dipolar coupled nuclear spins, Phys. Rev. A 74 (2006) 062312.
[38] R. Auccaise, J. Teles, R.S. Sarthour, T.J. Bonagamba, I.S. Oliveira, E.R. deAzevedo, A study of the relaxation dynamics in a quadrupolar NMR system using quantum state tomography, J. Mag. Res. 192 (2008) 17.
[39] R.R. Ernst, G. Bodenhausen, A. Wokaun, Principles of nuclear magnetic resonance in one and two dimensions, Oxford University Press, 1987.
[40] P. Dhiel, C.L. Khetrapal, NMR-Basic Principles and Progress, vol. 1, Springer-Verlag, New york, 1969.
[41] M.V. Berry, The adiabatic phase and Pancharatnam's phase for polarized light, J. Mod. Optics 34 (1987) 1401.
[42] B. Simon, Holonomy, the quantum adiabatic theorem and Berry's phase, Phys. Rev. Lett. 51 (1987) 2167.
[43] Y. Aharnov, J. Anandhan, Phase change during a cyclic quantum evolution, Phys. Rev. Lett. 58 (1987) 1593.
[44] D. Suter, G. Chingas, R.A. Harris, A. Pines, Berry's phase in magnetic resonance, Mol. Phys. 61 (1987) 1327.
[45] J.A. Jones, V. Vedral, A. Ekert, G. Castagnoli, Geometric quantum computation with NMR, Nature 403 (2000) 869.
[46] S.L. Zhu, Z.D. Wang, Implementation of universal quantum gates based on non-adiabatic geometric phases, Phys. Rev. Lett. 89 (2002) 97902.
[47] X.B. Wang, M. Keiji, Non-adiabatic geometric phase shift with NMR, Phys. Rev. Lett. 87 (2001) 097901.
[48] D. Suter, K.T. Mueller, A. Pines, Aharnov–Anandhan quantum phase by NMR interferometry, Phys. Rev. Lett. 60 (1988) 1218.
[49] R. Das, S.K. Karthick Kumar, A. Kumar, Use of non-adiabatic geometric phase for quantum computing by nuclear magnetic resonance, J. Magn. Reson. 177 (2005) 318.
[50] T. Gopinath, A. Kumar, Geometric quantum computation using fictitious spin-(1/2) subspaces of strongly dipolar coupled nuclear spins, Phys. Rev. A 73 (2006) 022326.
[51] R. Cleve, A. Ekert, C. Macchiavello, M. Mosca, Quantum algorithms revisited, Proc. R. Soc. Lond. A 454 (1998) 339.
[52] D. Collins, K.W. Kim, W.C. Holton, Deutsch–Jozsa algorithm as a test of quantum computation, Phys. Rev. A 58 (1998) 1633.
[53] O. Mangold, A. Heidebrecht, M. Mehring, NMR tomography of the three-qubit Deutsch–Jozsa algorithm, Phys. Rev. A 70 (2004) 042307.

[54] N. Linden, Herv Barjat and Ray Freeman an implementation of the DeutschJozsa algorithm on a three-qubit NMR quantum computer, Chem. Phys. Lett. 296 (1998) 61.
[55] R. Bruschweiler, Novel strategy for database searching in spin liouville Space by NMR ensemble computing, Phys. Rev. Lett. 85 (2000) 4815.
[56] F.M. Woodward, R. Bruschweiler, Solution of the Deutsch–Josza problem by NMR ensemble computing without sensitivity scaling, arXiv:quant-ph/0006024v2.
[57] R. Stadelhofer, D. Suter, W. Banzhaf, Quantum and classical parallelism in parity algorithms for ensemble quantum computers, Phys. Rev. A 71 (2005) 032345.